Laser Spectroscopic Study of Cold Host-Guest Complexes of Crown Ethers in the Gas Phase

Yoshiya Inokuchi[a], Ryoji Kusaka[a], Takayuki Ebata*[a], Oleg V. Boyarkin[b] and Thomas R. Rizzo*[b]

[a]Department of Chemistry, Graduate School of Science, Hiroshima University, Higashi-Hiroshima 739-8526, Japan

[b]Laboratoire de Chimie Physique Moléculaire, École Polytechnique Fédérale de Lausanne, Lausanne CH-1015, Switzerland

Laser spectroscopic study on the structure and dynamics of cold host-guest inclusion complexes of crown ethers (CEs) with various neutral and ionic species in the gas phase is presented. The complexes with neutral guest species are formed by using supersonic free jets, and those with ionic species are generated with an electrospray ionization (ESI) combined with a cold 22-pole ion trap. For CEs, various sizes of 3*n*-crown-*n*-ethers (*n* = 4, 5, 6 and 8) and their benzene-substituted species are used. For the guest species, we chose water, methanol, acetylene and phenol as neutral guest species, and for charged guest species, alkali metal cations are chosen. We measured electronic and vibrational spectra of the complexes by using various laser spectroscopic methods; electronic spectra for the neutral complexes are measured by laser-induced fluorescence (LIF). Discrimination of different species such as conformers is performed by

ultraviolet-ultraviolet hole-burning (UV-UV HB) spectroscopy. The vibrational spectra of selected species are observed by infrared-ultraviolet double resonance (IR-UV DR) spectroscopy. For the ionic complexes, ultraviolet photodissociation (UVPD) and IR-UV DR spectroscopy are applied. The complex structures are determined by comparing the observed spectra with those of possible structures obtained by density functional theory calculations. We discuss how the host CEs change their conformation or which conformer prefers to form unique inclusion complexes. These results tell us the key interactions for forming special complex, leading to the molecular recognition.

1. Introduction

Crown ethers (CEs) are cyclic ethers built with several oxyethylene (-CH_2-CH_2-O-) units, and are known to form inclusion complexes. In 1967, Pedersen discovered the first crown ether (CE), dibenzo-18-crown-6 (DB18C6), and investigated its complexation with metal salts [1,2] by using UV spectroscopy as one of three criteria to verify complex formation. CEs can include not only ionic species but also various neutral ones through non-covalent interactions, such as van der Waals (vdW) force and hydrogen(H)-bonding. Applications of crown ethers as molecular receptors, metal cation extraction agents, fluoroionophores and phase transfer catalytic media have been described in a number of studies in the literature. [3-14] One of the important aspects of CEs in the host/guest system is their selectivity of guest species.[9-14] For example, 18-crown-6 (18C6) forms an exceptionally stable 1:1 complex with K^+ compared to other alkali metal cations in

aqueous solution, [1,3] which is described by the best matching between the size of crown cavity and that of the spherical K^+. The metal ion–crown ether complexes were extensively investigated in the gas phase with mass spectrometric techniques, [15-27] and ion mobility methods [28,29]. It was found that the property of CEs in the gas phase is different from that in solution; 18C6 does not show a largest binding energy with K^+ among the alkali-metal cations.[17,25,27]

The discrepancy between the gas phase and solution results may come from two factors. First is a flexibility of the CE frame. Though the size of the cavity increases with an increase of *n* in 3*n*-crown-*n*, CEs become more flexible at the same time so that they can include different sizes of guest species by changing their conformations. For example, it is reported that dibenzeo-24-crown-8 (DB24C8), dibenzeo-30-crown-10 (DB30C10), and 30-crown-10 (30C10) can wrap a K^+ cation by folding their flexible crown rings. [30] Second is the effect of solvent molecules. It sometimes occurs that the most stable conformer in bare form is not the most sable one in solution, since the higher energy conformer can be largely stabilized by noncovalent interactions, such as dipole-dipole interaction and H-bonding with solvent molecules. Previous studies suggested that the water solvation to the complexes enhances the binding energy with K^+ [26,31].

Since it is difficult to investigate the guest/host interaction in the condensed phase excluding solvent effects, a stepwise study of the structures and energetics of clusters starting from the isolated molecule to micro-solvated complexes is essential. Recently, it has been demonstrated that the laser spectroscopic study of cold gas phase CEs and their complexes, not only for ionic species[32-43] but also the

neutral species[44-52], can provide a microscopic view on the structure and flexibility of CEs as well as micro-solvated effects under solvent-controlled conditions.

In the present study, we describe our spectroscopic study of the complexes of CEs with neutral[46-52] and ionic species[42,43] by using two methods to generate cold gas phase complexes; supersonic free jet expansion to generate neutral complexes and an electrospray ionization(ESI)/cold 22-pole ion trap to generate ionic complexes. The latter method is recently developed to study the structure of cations of nonvolatile molecular species, such amino acids, polypeptides, and their protonated species. [53-55] We apply variety of laser spectroscopic methods to these species. The ultraviolet (UV) spectra of bare molecules and their complexes are measured by using laser-induced fluorescence (LIF) or UV phtotodissociation (UVPD) spectroscopy. Discrimination of different species is performed by UV-UV hole-burning (HB) spectroscopy. The vibrational spectrum of each species is measured by infrared-ultraviolet double-resonance (IR-UV DR) spectroscopy. The combination of the supersonic free jet or ESI/cold 22-pole ion trap with the laser spectroscopic technique and a subsequent analysis by quantum chemical calculations results in a powerful tool to determine the structure and stability of the complexes.

We first describe the structures of the complexes with neutral complexes. The CEs we have chosen are dibenzo-18-crown-6 (DB18C6)[46,47,50,51], benzo-18-crown-6 (B18C6)[46,48], dibenzo-24-crown-8 (DB24C8)[49], and 3*n*-crown-*n* (*n* = 4, 5, 6 and 8). [52] The former three CEs have benzene chromophores and we generate the

complexes with rather simple guests; water, methanol, ammonia and acetylene. The interest of these systems is how the flexible nature of CEs affects the formation of inclusion complexes with the guest species having different shapes and binding characters, such as conformation change or preference. In the case of 3*n*-crwon-*n*, we generate the complexes with phenol, that is [3*n*-crwon-*n* – phenol] complexes, where phenol acts as a chromophore. The complexes are bound via several interactions, OH・・・O H-bonding, CH・・・π interaction, and dispersion force and we examine their contribution to form stable complexes and the size effect. All the complexes are formed under an isolated cold condition in the gas phase by supersonic free jet expansion. We measure their electronic spectra by LIF spectroscopy and infrared spectra by IR-UV DR spectroscopy. These spectra are compared with those of possible structures obtained by density functional theory (DFT) calculation, which enables us to determine the structures of the complexes. We finally discuss the structures of complexes between DB18C6 and alkali metal cations, M^+・DB18C6, where $M^+ = Li^+$, Na^+, K^+, Rb^+, and Cs^+.[42,43] The M^+・DB18C6 complexes are produced by nanoelectrospray, mass-selected by a quadrupole mass spectrometer and irradiated with a UV laser in a cold, 22-pole ion trap. We obtain the UV spectra of the M^+・DB18C6 complex ions by UVPD spectroscopy. Isolating and cooling the complexes in the gas phase greatly simplifies the UV spectra and provides well-resolved vibronic bands. Furthermore, we measure conformer-specific infrared spectra *via* IR-UV DR in the CH stretching (2800–3120 cm^{-1}) region. With an aid of DFT calculation, we determine the conformation of the complexes.

Based on these results, we shed light on the nature of the interaction between host and guest species and the mechanism of the inclusion process as well as the recognition of guest species.

2. Results and discussion

2.1 Inclusion complexes of benzene-substituted crown ethers with neutral guest species

Scheme 1

We first report the structure of DB18C6, B18C6, DB24C8 (scheme 1) and their complexes with neutral species, mostly water molecules. Though CEs are flexible, a substitution of benzene ring(s) in the crown frame makes the frame rigid because the –O–C=C–O– (where C=C represents the carbon atoms in the benzene ring) frame prefers a planar structure, which reduces the possible number of conformers. Another interesting aspect of this system is that the complexation with guest species may stabilize the CE conformation that is not stable in the monomer and the stabilization will depend on the guest species. We investigate how the structural flexibility affects the dynamics of the inclusion process at the microscopic level.

Figure 1.

Figure 1(a) shows the LIF spectrum of the S_1-S_0 transition of jet-cooled DB18C6 monomer and DB18C6-$(H_2O)_n$ complexes in the band origin region. [47] The UV-UV HB spectra obtained by monitoring bands **m1**, **m2**, **a**, and **c**-**f**, in Figure 1(b)-(h), indicate that each of the **m1**, **m2**, **a**, and **c**-**f** bands is assigned to the band origin

of different species. Bands **m1** and **m2** are attributed to the DB18C6 monomer, since they do not exhibit the OH stretching vibrations of water molecule(s) in the IR-UV DR spectra, though the spectra are not shown here. Transitions **a**-**f** are attributed to the band origins of the DB18C6-$(H_2O)_{n=1-4}$ complexes, because they exhibit OH stretching vibrations of water molecule(s) in the IR-UV DR spectra (See Figure 4). There are two characteristic features in the spectra of Figure 1. First is that **m1** shows a single peak, while **m2** exhibits doublet peaks with a separation of 5 cm^{-1}. The doublet structure is also observed in DB24C8[49] but not in B18C6[46], and is attributed to an exciton splitting[49] due to the interaction of the two benzene chromophores. The exciton splitting occurs due to the interaction of the dipole transitions of symmetrically equivalent chromophores, meaning the CE has C_i, C_2 or C_{2v} symmetry. In the case of C_2 or C_{2v} symmetry, the interaction appears as a doublet structure in the electronic spectrum, such as the splitting of **m2**. On the other hand, an appearance of a single peak, such as **m1**, indicates that the CE has a C_i symmetry or the two chromophores are not symmetrically equivalent with each other. Second characteristic feature is that all the transitions of the DB18C6-$(H_2O)_n$ complexes are blue-shifted with respect to the monomer bands and each band shows a doublet structure.

Figure 2.

The IR-UV DR spectra in the CH stretching region by monitoring bands **m1**, **m2** and **a** in the LIF spectrum (Figure 2(a)), are shown in Figure 2(b).[51] The bands in the 3000~3100 cm^{-1} region are assigned to the CH stretches of the benzene ring, and those in the 2800~3000 cm^{-1} region are due to the CH

stretching vibrations of the crown ring. As seen in Figure 2(b), the **m1** and **m2** show similar IR spectra with each other, indicating the two monomer, **m1** and **m2**, have a similar crown ring conformation with each other. On the other hand, the IR spectra of band **a** is different from them, indicating the DB18C6 part of the DB18C6-$(H_2O)_1$ complex (species **a**) has a different conformation from **m1** and **m2**. Figure 2(c) shows the simulated IR spectra for the energy optimized structures of DB18C6 and DB18C6-$(H_2O)_1$ complex, whose structures are shown in Figure 3. As seen in the spectra, the conformers (I)~(IV) show similar IR spectra with the observed ones of **m1** and **m2**. On the other hand, the IR spectrum of boat-DB18C6-$(H_2O)_1$ complex is very similar with the observed one of band **a**.

Figure 3

Figure 3(a) shows four lowest energy conformers and Figure 3(b) shows C_i and C_{2v} conformers of DB18C6 monomer.[51] It should be noted that the C_i and C_{2v} conformers have rather high energies so that they cannot be the candidates of the observed ones. This means that **m1 of** DB18C6, exhibiting a single peak, does not have C_i symmetry. Figure 3(c) shows the lowest energy structure of the DB18C6-$(H_2O)_1$ complex, in which DB18C6 has a boat structure with C_{2v} symmetry. Since the boat-DB18C6-$(H_2O)_1$ is the lowest energy structure and its IR spectrum reproduces the observed one of band **a** as described above, we conclude that the species of band **a** is the boat-DB18C6-$(H_2O)_1$ complex of Figure 3(c). For the DB18C6 monomer (**m1** and **m2**), it is difficult to determine the structures from the IR spectra alone. So, we obtained the electronic transition

energies for those conformers by TD-DFT calculation, which are shown in the right panel of Figure 3. From the comparison of the observed LIF spectrum and the calculated ones, **m1** is assigned to the conformer IV(C_1), and **m2** to the conformer II(C_2). Thus, the reason for an appearance of a single peak of **m1** is due to the fact that the two benzene chromophores are not symmetrically equivalent in IV(C_1). For **m2**, assigned to conformer II(C_2), the exciton splitting energy, ΔE, can be estimated by the following equation[47,56, 57],

$$\Delta E = 2 F V_{AB} \tag{1}$$

where

$$V_{AB} = \frac{\mu_A \mu_B}{4\pi\varepsilon_0 R_{AB}^3}\left(2\cos\theta_A \cos\theta_B - \sin\theta_A \sin\theta_B \cos\varphi \right). \tag{2}$$

R_{AB} is the distance between the centers of the two chromophores, θ_A and θ_B are the angles of the transition dipole moment with respect to the line connecting the two centers, and φ is the dihedral angle between the two transition dipoles. F is the vibrational part, which is determined by the Franck-Condon factor of the electronic transition. The transition dipole moment is calculated to be $\mu_A(=\mu_B)$ = 5.5 x 10^{-30} Cm from the oscillator strength of the S_1-S_0 electronic transition of 1,2-dimethoxybenzne (DMB) obtained by TD-DFT calculation. We use the values of θ_A, θ_B, φ, and R_{AB} to be 322°, 218°, 41°, and 0.87 nm, respectively, for the DFT calculated C_2 conformer (II). Substitution of these values to eq. (2) yields $2V_{AB}$= 64 cm^{-1}. This value is in good agreement with the TD-DFT calculated S_2-S_1 energy splitting for the C_2 conformer (II), 74 cm^{-1}, in Figure 3b. Though an estimation of F is difficult, we roughly estimated the value to be about 0.1 from the relative intensity of the (0, 0) band in the LIF spectrum

of Figure 1. This value and calculated $2V_{AB}$ gives ΔE = 6 cm^{-1} for the exciton splitting for the C_2 conformer (II) conformer, which shows an excellent agreement with the observed splitting of 5 cm^{-1}. This agreement of the splitting supports the assignment of the species **m2 to** the C_2 conformer.

From these results, it is concluded that DB18C6 takes the conformation of either conformer II (m2) or IV (m1) in the monomer but it changes to the boat conformer when it includes a water molecule in its cavity. Similar conformation change upon the complex formation or dimerization is reported in benzo-15-crown-5(B15C5)-$(H_2O)_n$ complexes [45] and other flexible molecules, where OH···O and OH···N play key interactions.[58, 59] The characteristics of the boat-DB18C6-$(H_2O)_1$ complex is that the water molecule in the cavity forms bidentate and bifurcated hydrogen-bond to O_1, O_3, O_4 and O_6 of DB18C6, which makes the boat conformation very stable.

Figure 4

The H-bonding structures of the DB18C6-$(H_2O)_n$ complexes with $n \geq 2$ are determined by the comparison of the observed IR-UV DR spectra with the simulated ones of the energy optimized structures. The spectra in the top panels of Figure 4 show the IR-UV DR spectra of the DB18C6-$(H_2O)_n$ complexes in the OH stretching region for the bands **a~f** of the LIF spectrum.[47] The stick diagrams are the simulated IR spectra of most probable species whose structures are shown in the lower panel of Figure 4. In the ***n***=1 complex, two isomers corresponding to bands **a** and **b** are presented. Band **a** is the major species and is assigned to the isomer 1W-1 having a bifurcated and bidentate

H-bonding. Band **b** is assigned to another bidentate H-bonding isomer (1W-2). Band **c** is assigned to the n = 2 complex, 2W-1. This complex has a structure in which a second water molecule (w2) is H-bonded to the bidentate water (w1) of 1W-1. Band **d** is assigned to the n = 3 complex (3W-1), in which three water molecules form bidentate H-bond. In this complex, one water (w1) forms a bifurcated and bidentate H-bonding at the bottom of the boat-DB18C6 and the other two water molecules (w2 and w3) form weaker bidentate H-bonds on the opposite (top) side of DB18C6. Bands **e** and **f** are assigned to the isomers of the n=4 complex, having a structure of 4W1-1 and 4W-2.

Thus, in all the DB18C6-$(H_2O)_n$ complexes DB18C6 takes the boat conformation and the H-bonding network of water molecules is built on this conformation. The conformation change or conformation preference upon the hydration is also found in other CEs. Figure 5 shows an example of such the conformation preference of B18C6. In the figure, the electronic spectrum of supersonically jet-cooled B18C6 and its change upon the addition of water vapor to the sample gas are demonstrated. [48] In the spectrum, four monomer conformers (M1~M4) are identified. By adding water vapor, band **D**, which corresponds to the structure M3, shows a large intensity among the isomers of the B18C6-$(H_2O)_1$ complex. Thus, B18C6 prefers this conformation upon the bidenate H-bonding with a water molecule. Zwier and coworkers also reported that "buckled" conformation of bare B15C5 and 4'-aminobenzo-15-crown-5 (ABC) molecule(s) changes their conformation to an open form in the presence of water molecule(s). [44,45]

Figure 5

2.2 Size-effect for forming a stable structure in the [3*n*-crown-*n*–phenol] complexes

In this section, we discuss the size dependence on the complex formation of 3*n*-crown-*n* (3*n*C*n*, *n* = 4, 5, 6, and 8) (scheme 2) with phenol, [3*n*-crown-*n* – phenol].

Scheme 2

In this system, phenol works as a chromophore of the complexes. The electronic transition energy is very sensitive to the conformer or isomer as shown in the previous section, and the bands with different conformer and isomer appear at different electronic transition energies, and we can discriminate them by applying UV-UV HB spectroscopy. Our interest of this system is to examine the synergetic effect of multiple interactions for the complex formation, such as OH···O H-bond, CH···π, and O···HC (aromatic) interactions. By changing *n* from *n* = 4 to 8, we investigate which size of 3*n*C*n* can form a uniquely stable complex with phenol.

Figure 6.

Figures 6(a)-(f) show the LIF (black curves) and UV-UV HB (blue curves) spectra of the diethyl ether (DEE)–phenol, 1,4-dioxane (DO)–phenol and 3*n*C*n*–phenol complexes.[52] The UV-UV HB spectra by fixing probe laser frequencies to major bands reproduce almost all the bands appearing in the LIF spectra, and the number of the isomers we identified for the complexes between phenol and ethers (DEE, DO, 12C4, 15C5, 18C6, and 24C8) is 1, 1, 3, 2, 1, and 2, respectively. Thus,

the number of the complexes dose not increase monotonically with the size of ethers. Especially, the appearance of only one isomer for the 18C6−phenol complex indicates a formation of a unique stable structure in this complex.

Figure 7.

Figure 7 shows IR-UV DR spectra of (a) phenol, (b) $(phenol)_2$, (c) phenol–H_2O, and (d)-(m) 3*n*C*n*–phenol complexes. In the spectra, bands in the 3300-3700 and 3000-3100 cm^{-1} regions are due to phenolic OH and CH stretching vibrations, respectively. [52] The OH stretching bands of all the ether–phenol complexes are red-shifted by 100~300 cm^{-1} with respect to phenol at 3657 cm^{-1}, meaning that the phenolic OH is H-bonded as a proton donor in these complexes. The low-frequency bands accompanied with the H-bonded OH stretch of the ether–phenol complexes [Figures 7(d)-(m)] are assigned to the intermolecular vibrations. The phenolic CH groups are classified into four groups at 3025, 3050, 3075 and 3100 cm^{-1}. Among them, the bands at ~3050 cm^{-1} are commonly observed for all the complexes. However, the intensities of the other bands in the 3*n*C*n*−phenol complexes, Figures 7(f)-(m), are much weaker than those of other complexes in Figures 7(a)-(e). In addition, a new band emerges at ~3070 cm^{-1} (marked by arrows) in the 3*n*C*n* − phenol complexes. Thus, the results indicate that the phenolic CH groups are also deeply involved in the complex formation.

Theoretical calculation supports the formation of one predominantly stable isomer for the 18C6–phenol complex. Table 1 lists the energies of the six lowest energy complexes for each of the 3*n*C*n*–phenol complexes. In the table, ΔE is the relative total energies and E_{int} is the intermolecular interaction energy

given by the following equation;

$$E_{int}(\text{CE-phenol}) = E(\text{CE-phenol}) - E(\text{CE}) - E(\text{phenol}) \qquad (3).$$

In this estimation the geometries of CE and phenol fragments are fixed to the ones the same as those in the CE–phenol complexes for E(CE) and E(phenol), and Zero-point-energy (ZPE) correction is not included. ΔE (CE) is the relative energy of CE part with respect to the most stable conformer. ΔG is the relative Gibbs energy of a complex at 298.15 K and 1 atm. We see that ΔE between the most stable (I) and the second stable isomers (II) of the 18C6-phenol complex (642 cm^{-1}) is much larger than those of the other three complexes with different n. We also see that the isomer (I) is most stable even at 298.15 K and 1 atm. Thus, the theoretical calculation predicts that only 18C6-phenol has one uniquely stable isomer compared to other 3nCn–phenol complexes. From the comparison of the values of E_{int} and ΔE (CE) among the complexes, the reason of the unique stabilization of 18C6–phenol can be attributed to its large interaction energy.

Figure 8.

Figure 8 shows the optimized structures of the three lowest-energy isomers of 3nCn-phenol complexes.[52] Blue dotted lines represent the O···HO ($\Delta r_{O\cdots H}$< 2.7 Å) and CH···π ($\Delta r_{H\cdots C}$ < 3.0 Å) interactions. In these complexes, a phenolic OH is H-bonded to ether O atom(s), and its π electrons interact with the crown CH group(s). In most of the 12C4– and 15C5–phenol isomers [Figures 8(a) and (b)], phenol interacts with crown CHs on one side of the phenyl ring. On the other hand, in the 18C6– and 24C8–phenol complexes [Figures 8(c) and (d)], the phenyl ring interacts with crown CHs on both sides. Especially in the three 24C8–phenol

isomers [Figure 8(d)], phenol is completely included in the 24C8 cavity via O···HO H-bond and four CH···π interactions, resulting in a large E_{int} (Table 1). The reason of the largest interaction energy for the conformer I of 18C6–phenol can be seen from the analysis of the conformation of 18C6 in the complex. Figure 8 also picks up the structures of the 18C6 part in the 18C6(I, II and III)–phenol complexes. In the 18C6(I) conformation, four oxygen atoms, O(1), O(4), O(10) and O(13) are directed toward the inside of the cavity, so that the phenol molecule collectively interacts with the four O atoms via bifurcated [O(1)···HO and O(4)···HO] H-bonding, CH···π, O(10)···HC(aromatic), and O(13)···HC(aromatic) interactions. On the other hand, in 18C6(II), O(4) is directed toward the outside of the cavity and H(3) hinders phenol from forming the bifurcated O···HO H-bond . Similarly in 18C6(III), O(13) is directed toward the outside of the cavity and H(12) hinders the O(13)···HC(aromatic) interaction. Thus, the shapes of phenol and 18C6(I) are best matched to have the largest E_{int} of the 18C6(I)-phenol complex via the collective intermolecular interactions consisting of O···HO, CH···π and O···HC(aromatic).

2.3 Structures of the [alkali metal ion•crown ether] inclusion complexes generated in cold 22-pole ion trap

Figure 9 displays the UVPD spectra of (a) room temperature K^+•DB18C6 and (b) K^+•DB18C6 that is cooled in the 22-pole ion trap.[42] The uncooled complex has a broad absorption around 36300 cm^{-1}. On the other hand, the UV spectrum of the cooled K^+•DB18C6 complex consists of many sharp bands, with the band

origin clearly observed at 36415 cm^{-1}. From the intensity and the vibrational frequency of hot bands observed on the low energy side of the band origin, we estimate the temperature of the cooled complex to be ~10 K. Comparison of the UV spectra in Figure 9 indicates that the broad absorption of the uncooled complex is mainly due to thermal congestion.

Figure 9.

The left panel of Figure 10 shows the UVPD spectra of the cooled M^+•DB18C6 (M = Li, Na, K, Rb, and Cs) complexes in the 35500–38000 cm^{-1} region[42] together with the LIF spectrum of jet-cooled DB18C6 monomer. Recently, Kim and coworkers also reported similar UV spectra of these complexes by using cold quadrupole ion trap.[41] All the M^+•DB18C6 complexes show a blue shift of the absorption relative to uncomplexed DB18C6. The blue-shift of the S_1-S_0 electronic transition is also observed in the M^+•DMB, M^+•B18C6 and M^+•B15C5 complexes[60] and even in the DB18C6-$(H_2O)_n$ complexes (Figure 1). In Figure 10, the Li^+ complex shows the most blue-shifted band origin, indicating the strongest interaction. This result is consistent with enthalpies of binding measured by collision-induced dissociation.[27] For the Rb^+ and Cs^+ complexes, the band origin gradually shifts to the red with respect to the position of the K^+ complex; the interaction between DB18C6 and the metal ion becomes progressively weaker from K^+ to Cs^+. In the spectra of the Li^+ and Na^+ complexes, the origin band is weak, and low-frequency progressions are very extensive and intense. In contrast, the K^+, Rb^+, and Cs^+ complexes show strong origin bands. These results indicate that the structural change upon the S_1–S_0 excitation is relatively larger for the Li^+

and Na^+ complexes.

Figure 10.

The right panel in Figure 10 displays expanded views of the UVPD spectra of the K^+•DB18C6, Rb^+•DB18C6, and Cs^+•DB18C6 complexes around their respective band origins. [42] As is highlighted by solid lines, the spectral features exhibit a band splitting of a few cm^{-1}. From the study of UV spectroscopy for jet-cooled DB18C6 describe previously, we assign this structure to the exciton splitting due to the interaction between the benzene chromophores. The doublet structure appears repeatedly in the spectra, built on top of vibrational progressions of ~20 and 47 cm^{-1}, which are due to low-frequency vibrations of the complexes (labeled α and β in Figure 10). All the UVPD spectra in Figure 10 have a number of vibronically resolved bands. In order to distinguish vibronic bands due to different conformers, IR-UV DR spectra are measured by monitoring strong vibronic bands.

Figure 11 shows the IR-UV DR spectra of the M^+•DB18C6 complexes in the CH stretching (2800–3120 cm^{-1}) region. [42] For the Li^+ and Na^+ complexes, two kinds of IR spectra are obtained; the IR-UV spectra in Figures. 11a–d are measured by monitoring the intensity of the vibronic bands labeled Li-I, Li-II, Na-I, and Na-II in Figure. 10. These results indicate that there exist at least two isomers for the Li^+ and Na^+ complexes. The IR-UV spectra of the K^+, Rb^+, and Cs^+ complexes in Figures 11e–g are observed by monitoring the origin band (K-I, Rb-I, and Cs-I in Figure 10). Using other vibronic bands of these complexes produces the same IR spectra, demonstrating that there is only one stable isomer for each

of them. The similarity of the IR spectra of the K^+, Rb^+, and Cs^+ complexes imply that the conformation of DB18C6 in each of them will be similar.

Figure 11.

The structures of the M^+•DB18C6 complexes were determined with the aid of DFT and TD-DFT calculations. Figure 12 displays the lowest-energy structures calculated at the M05-2X/6-31+G(d) level. The Li^+ and Na^+ complex have highly distorted forms. In the K^+, Rb^+, and Cs^+ complexes, on the other hand, the ether ring of DB18C6 opens the most, adopting a boat (C_{2v}) conformation.

Figure 12.

The K^+ ion is in the center of the cavity, while the Rb^+ and Cs^+ ions sit on top of the open cavity because their ion diameters are larger than the cavity size. Figure 13 shows a comparison of the observed UV spectra of the M^+•DB18C6 complexes and the TD-DFT calculated electronic transition energies at the M05-2X/6-31+G(d) level. Here the electronic transition energies are scaled with a factor of 0.8340, which is adapted so as to reproduce the transition energy of the origin band of K^+•DB18C6. We see that the calculation well predicts the observed blue-shift of the electronic transition energy with increasing the size of the M^+ guest and the transition energies of different isomers. In these complexes, M^+ is bound to the α-Oxygen(s) of dimethoxy benzene. The blue-shift of the electronic transition with respect to uncomplexed species means that the interaction between M^+ and α-Oxygen becomes weaker upon the electronic excitation to the S_1 state. Actually, the distance between the center of the benzene rings was calculated for the K^+•DB18C6 complexes, and it was found that the distance in S_1 is longer than that in S_0 and the difference is larger of the smaller size M^+.

Figure 13.

We can compare the gas-phase structures in Figure 12 with those determined by X-ray diffraction analysis in crystals or by IR and NMR spectroscopy in solution. The Cambridge Structural Database (CSD ver. 5.31) of the Cambridge Crystallographic Data Centre[61] contains 32, 59, 10, and 3 crystal structures for the Na^+, K^+, Rb^+, and Cs^+ complexes, respectively. No crystal data of the Li^+•DB18C6 complex was put into the database. Rb^+ and Cs^+ ions are each held by two DB18C6 molecules in all the crystals, implying that they are too large to be located inside the DB18C6 cavity. For all the K^+ complexes in crystals, the DB18C6 part has a boat-type open form.[62,63] The Na^+•DB18C6 complexes in crystals also have similar boat-type structures; counter ions take part in the coordination of the Na^+ cations, which significantly influences the complex structure.[64-67] The IR and NMR studies in solution suggested that the K^+•DB18C6 and Na^+•DB18C6 complexes have similar conformations from each other.[68,69] In contrast, the Na^+ and K^+ complexes take quite different forms in the gas phase (Figure 12). The K^+•DB18C6 complex takes a boat conformation, similar to those in crystals and in solution. For the Na^+•DB18C6 complex in the gas phase, however, the ether ring is highly distorted to fit the cavity size to Na^+. These results indicate that the solvent plays crucial roles for the complex structure in the condensed phase.

Conclusion

In this review, we reported our study on the structure of inclusion

complexes of crown ethers with various guest species in the gas phase. By using cooling effect either by supersonic free jet expansion or ESI/cold22-pole ion trap, well-resolved electronic and vibrational spectra of conformer and isomer-selected complexes were obtained. In the complexes of benzene substituted crown ethers (B18C6, DB18C6, and DB24C8) with simple polyatomic molecules, we found the CEs change their conformation to form the most stable complex, and a bidentate (and sometimes bifurcated) H-bonding is a key interaction for such the conformation change. In the case of 3*n* -crown-*n*–phenol complex system, the complexes are bound by multiple intermolecular interactions, which work synergetically to form very stable complexes. For the alkali metal ion・DB18C6 complexes, their UV spectra show extensive low frequency vibrations. A clear size dependence was identified for including the metal ions in the cavity; for including Li^+ or Na^+, DB18C6 distorts the ether ring to fit the cavity size to the ion diameter. For K^+, DB18C6 opens the cavity the most and the K^+ ion fits well inside. For Rb^+ and Cs^+, DB18C6 takes an open form similar to the K^+・DB18C6 complex. However, since the ion size is too large to fit inside the cavity of DB18C6, the ion sits on top of the ether ring. All these results show an importance of the flexibility of CEs for forming stable inclusion complexes with guest species, regardless the guest is ion or neutral.

As to the future work, we will extend this study to M^+・DB18C6・$(H_2O)_n$ complexes to challenge the problem of size recognition of alkali-metal ions in aqueous solution. Such a study has been recently reported by Rodriguez and Lisy for the M^+・18C6・$(H_2O)_{1-4}$ complexes by IR spectroscopy.[18,20] The structures

they proposed for hydrated $Rb^+ \cdot 18C6$ and $Cs^+ \cdot 18C6$ complexes are consistent with what one might expect from the structures of the $M^+ \cdot B18C6$ and $M^+ \cdot DB18C6$ complexes determined in this study, that is H_2O molecules are bound on the open side of the complexes. On the other hand, for $Li^+ \cdot 18C6$ and $Na^+ \cdot 18C6$, they proposed that addition of one H_2O molecule opens the ether rings, which would represent a significant change in structure of the bare complexes. One problem in their study is that there remains ambiguity in the number (n) and structure (conformer) of the $M^+ \cdot 18C6 \cdot (H_2O)_n$ complexes because only IR spectroscopy is applied. Since we can determine the number and discriminate the conformers for the $M^+ \cdot DB18C6 \cdot (H_2O)_n$ complexes by the double resonance approach, the study to the hydrated crown ether complexes should allow us for further clarification in the selective capture of crown ethers in solution.

Experimental Section

Spectroscopy Measurements

Details of the experiment were described in our previous papers.[42,43,46-53] For generating gas phase cold molecules and complexes of crown ethers, a supersonic free jet expansion by using pulsed nozzle was used in Hiroshima University. The pulsed nozzle consists of a commercially available valve and a sample housing made of polyimide resin. The sample housing that contains the sample powder is attached to the head of the valve and it is heated to ~400 K to evaporate the nonvolatile sample. The housing has a 1 mm orifice at the exit. The poppet of the pulsed valve, which is also made of polyimide resin, is extended to

the orifice of the sample housing and controls the injection of the sample gas. The gaseous mixture of the sample (B18C6, DB18C6, or DB24C8) and guest molecules, premixed with helium carrier gas at a total pressure of 3 bar, is expanded into the vacuum chamber through the orifice. For generating 3*n*-crown-*n* –phenol complexes, a gas mixture of 3*n*-crown-*n* (12C4, 15C5, 18C6, or 24C8 heated at 40, 50, 80, 90 °C, respectively), phenol, and helium was expanded into vacuum through a pulsed nozzle. For the generation of diethyl ether (DEE)-phenol or 1,4-dioxane (DO)-phenol complexes, liquid DEE or DO was put in a stainless steel bottle connected to a gas line. The partial pressure of DEE and DO was controlled by a thermo regulator. For the LIF measurement, an output of a pulsed UV laser (Inrad, Autotracker III (BBO) / Lambda Physik, Scanmate / Continuum, Surelite II) was introduced to the vacuum chamber at ~30 mm downstream of the nozzle. LIF spectra were obtained by detecting the fluorescence as a function of UV frequency. In UV-UV HB spectroscopy, two UV lasers were used; pump and probe lasers. The frequency of the probe UV laser was fixed to a vibronic band of a specific species and its fluorescence signal was monitored. A pump UV laser (Inrad, Autotacker II (KDP)/ Continuum, ND6000/ Continuum, Surelite II) was introduced to the jet at ~10 mm upstream of the probe laser beam. The pump light was introduced ~4 μs prior to the probe one. When the pump laser frequency is resonant to a transition of the monitored species, the species is excited to the upper level, resulting in the depletion of the fluorescence signal monitored by the probe light. Thus, the electronic spectrum of the monitored species is obtained as a fluorescence dip spectrum as a function of the pump UV frequency. The

experimental scheme of IR-UV DR spectroscopy for measuring infrared spectra is similar to that of UV-UV HB spectroscopy. An output of a tunable IR laser (Laser Vision/ Quanta-Ray, GCR250) was introduced coaxially with the UV probe laser with its frequency fixed to a vibronic band. The IR laser was irradiated at ~100 ns prior to the probe UV. The frequency of the IR pump laser was scanned while monitoring the fluorescence signal. The depletion of the fluorescence occurs when the IR frequency is resonant to vibrational transitions of the monitored species. Thus, IR spectrum in the S_0 state is obtained as a fluorescence dip spectrum.

The ESI/Cold 22-pole ion trap - laser spectroscopic measurement was performed by using a machine in École Polytechnique Fédérale de Lausanne.[42,43,53] The $M^+ \bullet$DB18C6 (M =Li, Na, K, Rb, and Cs) complexes are produced continuously at atmospheric pressure via nanoelectrospray, mass-selected in a quadrupole mass filter, and injected into a 22-pole RF ion trap, which is cooled by a closed cycle He refrigerator to 4 K. The trapped ions are cooled internally and translationally to ~10 K through collisions with cold He buffer gas, which is pulsed into the trap. The trapped ions are then irradiated with a UV laser pulse, which causes some fraction of them to dissociate. The resulting charged photofragments, as well as the remaining parent ions, are released from the trap, mass-analyzed by a quadrupole mass filter, and detected with a Channeltron electron multiplier. Ultraviolet photodissociation (UVPD) spectra of parent ions are obtained by plotting the yield of a particular photofragment ion as a function of the wavenumber of the UV laser. For IR-UV DR spectroscopy, the output of an IR OPO counter-propagates collinearly with the UV pulse, arriving in the trap

~100 ns prior to it. The wavenumber of the UV laser is fixed to a particular vibronic band in the electronic spectra for monitoring the population of a conformer and the wavenumber of the OPO is scanned while monitoring fragment ion intensity induced by the UV laser. Conformer-specific IR spectra are obtained by plotting the yield of a particular photofragment as a function of the OPO wavenumber. For distinguishing vibronic bands due to different conformers, we measure UVPD spectra with the OPO wavenumber fixed to a particular vibrational band.

Computational

For a broad structural survey of the isomers for the complexes of crown ethers, we first carried out Monte Carlo simulation by mixed torsional search with low-mode sampling [70] in MacroModel V.9.1[71] with MMFF94s force field,[72] and optimized the geometries by PRCG algorithm with a convergence threshold of 0.05 kJ/mol. In order to eliminate redundant conformations from the optimized geometries, the maximum distance threshold was set to 0.5–1.0 Å. For the DB18C6 complexes, 200 conformers were obtained at within 20 kJ/mol energy. In the case of 3*n*C*n*-phenol complexes, 300-1000 isomers were obtained for each 3*n*C*n*-phenol complex within 20 kJ/mol energy. For $M^+ \bullet$ B18C6 complexes, 219, 201, 123, 109, and 83 conformations are found for the Li^+, Na^+, K^+, Rb^+, and Cs^+ complexes, respectively, within 41.84 kJ/mol energy. All the isomers were optimized by density functional theory (DFT) calculation at B3LYP/6-31+G* or M05-2X/6-31+G* level with *loose* optimization criteria using GAUSSIAN 09

program package.[73] 20 low-lying isomers were re-optimized for each complex at ωB97X-D/6-31++G** level with *tight* optimization criteria and *ultrafine* grid. The total energy was corrected by non-scaled zero-point vibrational energy (ZPE). The oscillator strength and transition energy of electronic transitions are obtained with time-dependent DFT (TD-DFT) at the B3LYP/6-31+G* or M05-2X/6-31+G* level. The obtained vibrational and electronic transition frequencies were scaled, which depend on the level of calculation. For the DB18C6 complexes, the scaling factors were 0.9270 and 0.83576 for vibrational and electronic transition energies, respectively, at M05-2X/6-31+G* level.

Acknowledgement

This study is supported by JSPS through the program “Strategic Young Researcher Overseas Visit Program for Accelerating Brain Circulation”.

References

1. C. J. Pedersen, *J. Am. Chem. Soc.* **1967,** *89*, 7017-7036.

2. C. J. Pedersen, *Science* **1988,** *241*, 536-540.

3. A. M. Stuart, J. A. Vidal, *J. Org. Chem.* **2007**, *72*, 3735-3740.

4. N. Jose, S. Sengupta, J. K. Basu, *J. Mol. Catal. A: Chem.* **2009**, *309*, 153-158.

5. J. Malval, I. Gosse, J. Morand, R. Lapouyade, *J. Am. Chem. Soc.* **2002**, *124*, 904-905.

6. R. M. Uda, T. Matsui, M. Oue, K. Kimura, *J. Inclusion Phenom. Macrocyclic Chem.* **2005**, *51*, 111-114.

7. I. F. Uchegbu, S. P. Vyas, *Int. J. Pharm.* **1998**, *172*, 33-70.

8. L. Tavano, R. Muzzalupo, S. Trombino, I. Nicotera, C. O. Rossi, C. L. Mesa, *Colloids Surf. B*, **2008**, *61*, 30-38.

9. R. M. Izatt, J. H. Rytting, D. P. Nelson, B. L. Hayamore, J. J. Christensen, *Science*, **1969**, *164*, 443-444.

10. R. M. Izatt, D. P. Nelson, J. H. Rytting, J. J. Christensen, *J. Am. Chem. Soc.* **1971**, *93*, 1619-1623.

11. C. J. Pedersen, H. K. Frensdorff, *Angew. Chem. Int. Ed.* **1972**, *11*, 16-25.

12. R. M. Izatt, R. E. Terry, B. L. Haymore, L. D. Hansen, N. K. Dalley, A. G. Avondet, J. J. Christensen, *J. Am. Chem. Soc.* **1976**, *98*, 7620-7626.

13. R. M. Izatt, R. E. Terry, D. P. Nelson, Y. Chan, D. J. Eatough, J. S. Bradshaw, L. D. Hansen, J. J. Christensen, *J. Am. Chem. Soc.* **1976**, *98*, 7626-30.

14. J. D. Lamb, R. M. Izatt, C. S. Swain, J. J. Christensen, *J. Am. Chem. Soc.* **1980**, *102*, 475-479.

15. H. Zhang, J. H. Chu, S. Leming, D. V.Dearden, *J. Am. Chem. Soc.* **1991,** *113* (19), 7415-7417.

16. H. Zhang, D. V. Dearden, *J. Am. Chem. Soc.* **1992,** *114* , 2754-2755.

17. S. Maleknia, J. Brodbelt, *J. Am. Chem. Soc.* **1992,** *114* , 4295-4298.

18. I. H. Chu, H. Zhang, D. V.Dearden, *J. Am. Chem. Soc.* **1993,** *115* , 5736-5744.

19. J. S. Brodbelt, C. C. Liou, *Pure Appl. Chem.* **1993,** *65* , 409-414.

20. D. V. Dearden, H. Zhang, I. H. Chu, P. Wong, Q. Z. Chen, *Pure Appl. Chem.* **1993,** *65*, 423-428.

21. D. Ray, D. Feller, M. B. More, E. D. Glendening, P. B. Armentrout, *J. Phys. Chem.-Us* **1996,** *100* , 16116-16125.

22. F. Sobott, W. Kleinekofort, B. Brutschy, , *Anal. Chem.* **1997,** *69*, 3587-3594.

23. M. B. More, D. Ray, P. B. Armentrout, *J. Phys. Chem. A* **1997,** *101*, 4254-4262.

24. M. B. More,; D. Ray,; P. B. Armentrout, ulsen, D. V. Dearden, *Int. J. Mass Spectrom.* **2003,** *227*, 63-76.

25. M. B. More, D. Ray, P. B. Armentrout, *J. Am. Chem. Soc.* **1999,** *121*, 417-423.

26. P. B. Armentrout, *Int. J. Mass Spectrom.* **1999,** *193*, 227-240.

27. J. D. Anderson, E. S. Paulsen, D. V. Dearden, *Int. J. Mass Spectrom.* **2003,** *227*, 63-76.

28. S. Lee, T. Wyttenbach, G. Vonhelden, M. T. Bowers, *J. Am. Chem. Soc.* **1995,** *117*, 10159-10160.

29. T. Wyttenbach, G. von Helden, M. T. Bowers, *Int. J. Mass Spectrom.* **1997,** *165*, 377-390.

30. J. W. Steed, J. L. Atwood, *Supramoleuclar Chemsitry*, 2nd ed., **2009**, John

Wiley & Sons, Ltd., West Sussex, UK

31. D. Feller, *J. Phys. Chem. A*, **1997**, 101, 2723-2731

32. J. D. Rodriguez, T. D. Vaden, J. M. Lisy, *J. Am. Chem. Soc.* **2009,** *131*, 17277-17285.

33. J. D. Rodriguez, J. M. Lisy, *J. Phys. Chem. A* **2009,** *113* , 6462-6467.

34. J. D. Rodriguez, J. M. Lisy, *Int. J. Mass Spectrom.* **2009,** *283* , 135-139.

35. J. D. Rodriguez, D. Kim,; P. Tarakeshwar, J. M. Lisy, *J. Phys. Chem. A* **2010,** *114* , 1514-1520.

36. B. Martinez-Haya, P. Hurtado, A. R. Hortal, J. D. Steill, J. Oomens, P. J. Merkling, *J. Phys. Chem. A* **2009,** *113*, 7748-7752.

37. B. Martinez-Haya, P. Hurtado, A. R. Hortal, S. Hamad, J. D. Steill, J. Oomens, , *J. Phys. Chem. A* **2010,** *114* , 7048-7054.

38. P. Hurtado, A. R. Hortal, F. Gámez, S. Hamad,; B. Martínez-Haya, *Phys. Chem. Chem. Phys.* **2010,** *12*, 13752-13758.

39. C. M. Choi,; H. J. Kim, J. H. Lee, W. J. Shin, T. O. Yoon, N. J. Kim, J. Heo, *J. Phys. Chem. A* **2009,** *113* , 8343-8350.

40. C. M. Choi, J. H. Lee, Y. H. Choi, H. J. Kim, N. J. Kim,;J. Heo, , *J. Phys. Chem. A* **2010,** *114* , 11167-11174.

41. C. M. Choi, D. H. Choi, J. Heo, N. J. Kim, S. K. Kim, *Angew. Chemie Int. Ed.* **2012,** *51*, 7297-7300.

42. Y. Inokuchi, O. V. Boyarkin, R. Kusaka, T. Haino, T. Ebata, T. R. Rizzo, *J. Am. Chem. Soc.* **2011,** *133* , 12256-12263.

43. Y. Inokuchi, O. V. Boyarkin, R. Kusaka, T. Haino, T. Ebata, T. R. Rizzo, *J. Phys. Chem. A* **2012**, 116, 4057-4068.

44. V. A. Shubert, W. H. James, T. S. Zwier, *J. Phys. Chem. A* **2009,** *113*, 8055-8066.

45. V. A. Shubert, C. W. Muller, T. S. Zwier, *J. Phys. Chem. A* **2009,** *113*, 8067-8079.

46. R. Kusaka, Y. Inokuchi, T. Ebata, *Phys. Chem. Chem. Phys.* **2007,** *9*, 4452-4459.

47. R. Kusaka, Y. Inokuchi, T. Ebata, *Phys. Chem. Chem. Phys.* **2008,** *10*, 6238-6244.

48. R.Kusaka, Y. Inokuchi, T. Ebata, , *Phys. Chem. Chem. Phys.* **2009,** *11*, 9132-9140.

49. S. Kokubu, R. Kusaka, Y. Inokuchi, T. Haino, T. Ebata, *Phys. Chem. Chem. Phys.* **2010,** *12* , 3559-3565.

50. R. Kusaka,; Y. Inokuchi,; S. S. Xantheas,; T. Ebata, *Sensors,* **2010,** *10*, 3519-3548.

51. R. Kusaka, S. Kokubu, Y. Inokuchi, T. Haino, T. Ebata, *Phys. Chem. Chem. Phys.*, **2011**, *13*, 6827-6836

52. R. Kusaka, Y. Inokuchi, T. Haino, T. Ebata, *J. Phys. Chem. Letters*, **2012**, *3*, 1414–1420

53. O. V. Boyarkin, S. R. Mercier, A. Kamariotis, T. R. Rizzo, *J. Am. Chem. Soc.* **2006**, 128, 2816-2817

54. T. R. Rizzo, J. A. Stearns, O. V. Boyarkin, I*nt. Rev. Phys. Chem.* **2009**, *28*, 481-515

55. N. S. Nagornova, T. R. Rizzo, O. V. Boyarkin, *Science*, **2012,** *336*, 320-323

56. A. Müller, F. Talbot, S. Leutwyer, *J. Chem. Phys.* **2002**, *116*, 2836-2844

57. P. Ottiger, S. Leutwyer, H. Köppel, *J. Chem. Phys.,* **2012**, *136*, 174308 (13 pages)

58. K. Le Barbu, F. Lahmani, A. Zehnacker-Rentien, *J. Phys. Chem.* **A 2002**, *106*, 6271-6278

59. J. J. Lee, S. Hesse, M. A. Suhm, *J. Mol. Struct.* **2010**, *976*, 397-404

60. Y. Inokuchi, O. V. Boyarkin, R. Kusaka, T. Haino, T. Ebata, T. R. Rizzo, *J. Phys. Chem.* **A 2012**, *116*, 4057-4068

61. F. H. Allen, *Acta Crystallogr. Sect. B-Struct. Commun.* **2002,** *58*, 380-388.

62. N. S.Poonia, M. R. Truter, *J. Chem. Soc.-Dalton Trans.* **1973,** *19*, 2062-2065.

63. A. Bianchi, J. Giusti, P. Paoletti, S. Mangani, *Inorg. Chim. Acta* **1986,** *117*, 157-164.

64. D. Bright, M. R.Truter, *Nature* **1970,** *225*, 176-177.

65. D. Bright, M. R. Truter, *J. Chem. Soc. B* **1970,** (8), 1544-1550.

66. M. A. Bush, M. R.Truter, *J. Chem. Soc. D* **1970,** (21), 1439-1440.

67. M. A. Bush, M. R. Truter, *J. Chem. Soc. B* **1971,** (7), 1440-1446.

68. D. Live, S. I. Chan, *J. Am. Chem. Soc.* **1976**, *98*, 3769-3778.

69. A. T. Tsatsas, R. W. Stearns, W. M. Risen, Jr., *J. Am. Chem. Soc.* **1972**, *94*, 5247-5253.

70. I. Kolossváry, W. C. Guida, *J. Am. Chem. Soc.* **1996**, *118*, 5011-5019.

71. MacroModel, version 9.1, Schrödinger, LLC, New York, NY, 2005.

72. T. A. Halgren, *J. Comput. Chem.* **1999**, *20*, 730-748.

73. M. J. Frisch, G. W. Trucks, H. B. Schlegel, G. E. Scuseria, M. A. Robb, J. R. Cheeseman, G. Scalmani, V. Barone, B. Mennucci, G. A. Petersson, *et al.* Gaussian 09, revision A.02; Gaussian, Inc.: Wallingford, CT, **2009**

Table 1 Relative total (ΔE) and intermolecular interaction (E_{int}) energies of the six most stable isomers of 3*n*C*n*-phenol 1:1 complexes optimized at ωB97X-D/6-31++G** level. ΔE(CE) is relative energy of the conformation of crown part in each complex. ΔG is relative Gibbs energy of a complex at 298.15 K and 1 atm. All the values are in cm^{-1} unit.

	12C4 (*n*=4)				15C5 (*n*=5)				18C6 (*n*=6)				24C8 (*n*=8)			
	ΔE	E_{int}	ΔE(CE)	ΔG	ΔE	E_{int}	ΔE(CE)	ΔG	ΔE	E_{int}	ΔE(CE)	ΔG	ΔE	E_{int}	ΔE(CE)	ΔG
I	0	5939	186	0	0	6872	507	381	0	8354	265	0	0	10157	1225	0
II	43	6007	303	87	16	7175	961	294	642	7965	351	812	124	9806	844	72
III	88	5859	124	171	74	6129	0	0	684	7710	179	552	419	9730	929	628
IV	99	5727	0	253	197	6447	283	583	872	7426	0	1047	586	8692	0	790
V	183	5963	333	277	220	7102	967	479	951	7352	134	736	623	9303	891	581
VI	280	5870	328	508	375	6304	331	596	991	7672	379	955	677	9240	863	592

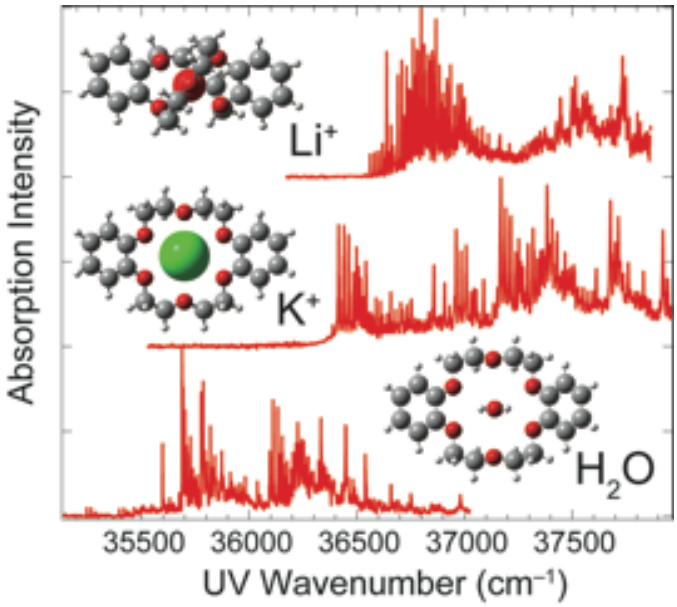

Graphic abstract:

Cold host-guest complexes of crown ethers in the gas phase:

The structure of cold inclusion complexes of crown ethers (CEs) with various neutral and ionic species in the gas phase is reported. By the combination of laser spectroscopy and theoretical analysis, a detail of the interaction energy and importance of flexibility of CEs for the formation of unique complex structure as well as molecular recognition are discussed.

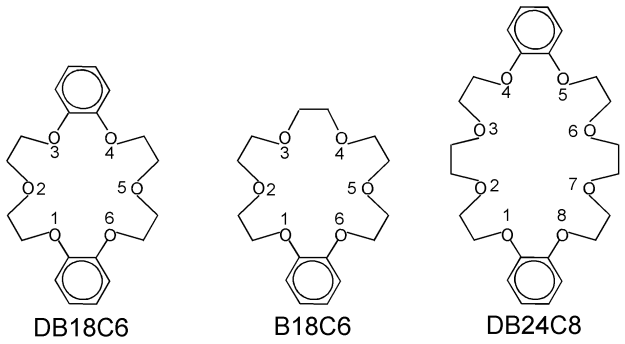

Scheme 1

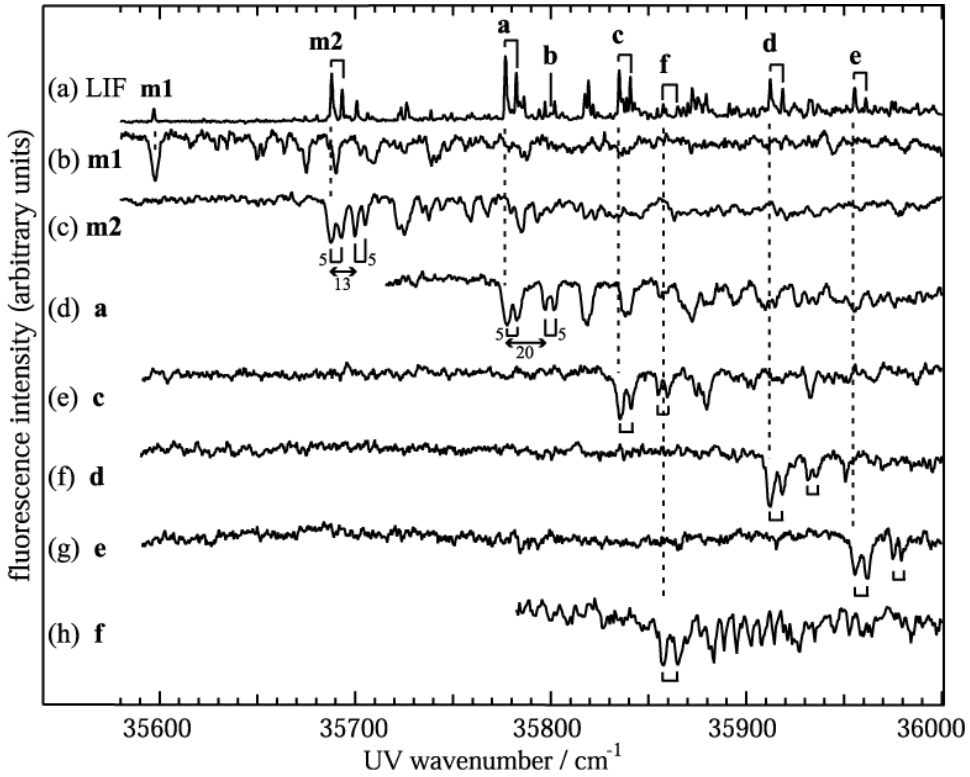

Figure 1. (a)LIF spectrum of jet-cooled DB18C6 and its hydrated complexes. (b)-(h) UV-UV HB spectra measured by monitoring bands **m1**, **m2**, **a**, and **c**-**f** in the LIF spectrum, respectively. The numbers in (c) and (d) show the energy interval (cm^{-1}) in the corresponding regions. Figure adapted from (Ref. 47)

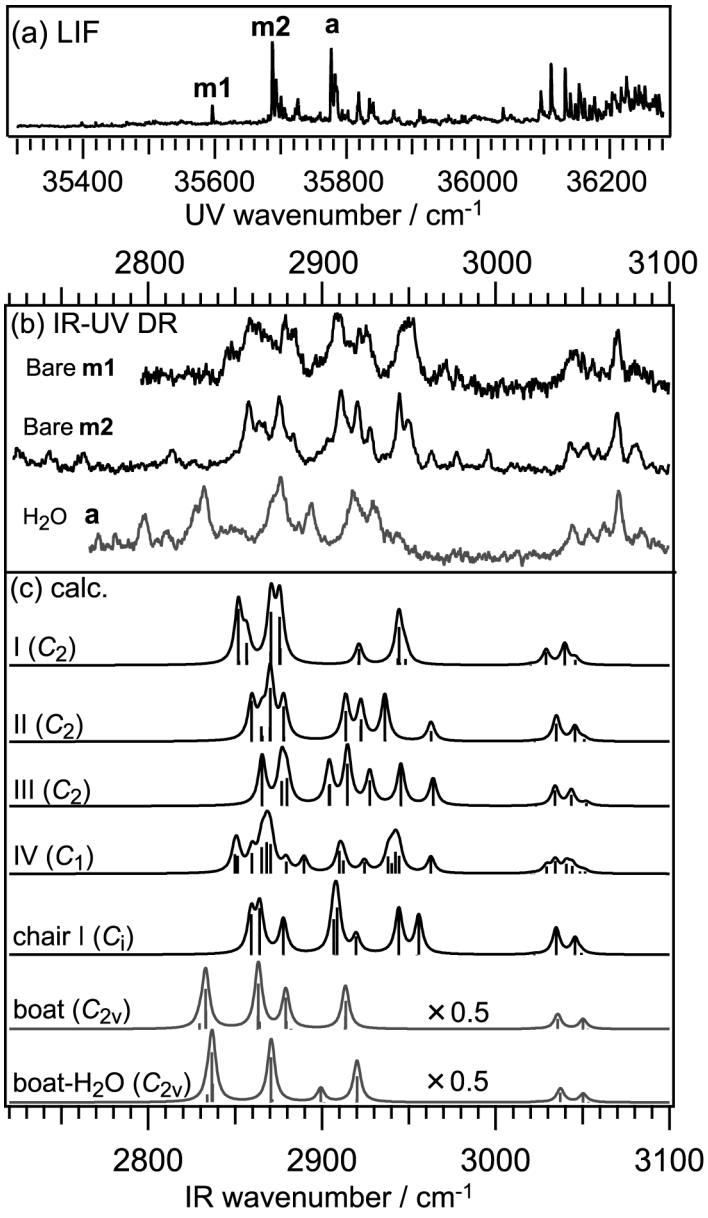

Figure 2. (a) LIF spectrum of bare DB18C6 (**m1** and **m2**) and DB18C6-H_2O (species **a**). (b) IR-UV DR spectra of **m1**, **m2**, and **a**. (c) Calculated IR spectra of optimized bare DB18C6 and DB18C6-H_2O at M05-2X/6-31+G* level. The optimized geometries are shown in Figure 3. Figure adapted from Kusaka et al. (Ref. 51)

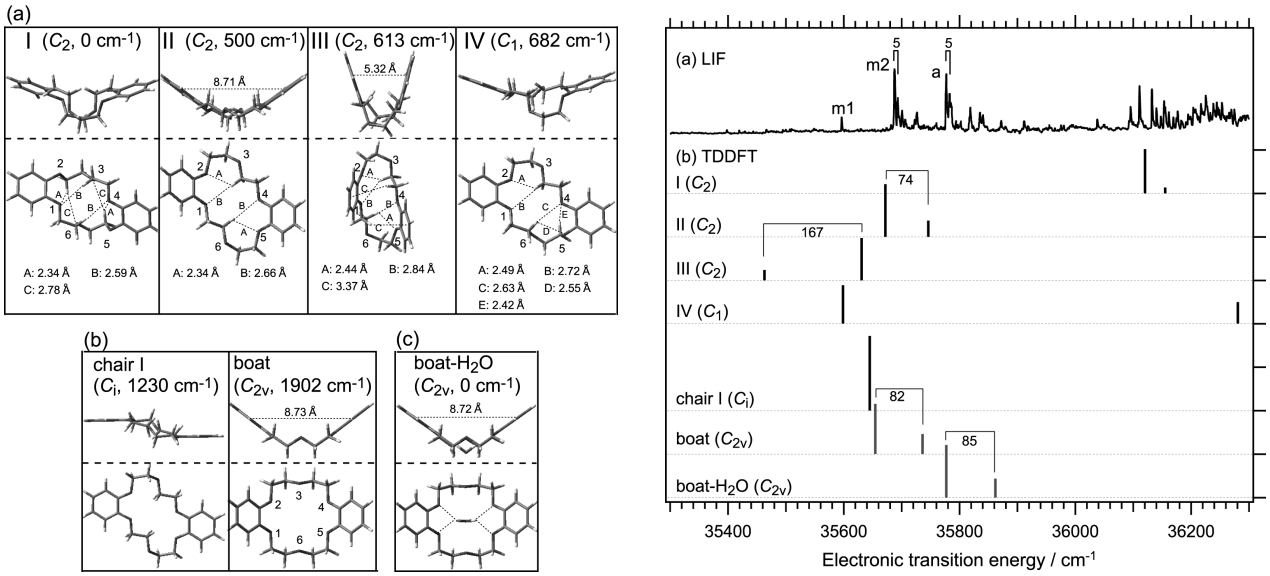

Figure 3 (Left) Optimized structures of bare DB18C6 and DB18C6-H_2O. (a) four most stable structures of DB18C6, (b) DB18C6 (chair I and boat), and (c) DB18C6-H_2O (boat-H_2O). Relative energies with respect to the most stable structure are displayed in cm^{-1} unit. The distances of CH···O, CH···π and π···π are also indicated. (Right) (a) LIF spectrum of bare DB18C6 and DB18C6-H_2O. (b) S_1-S_0 and S_2-S_0 electronic transition energies (bar graph) obtained by TDDFT calculations at the M05-2X/6-31+G* level. Figure adapted from (Ref. 51)

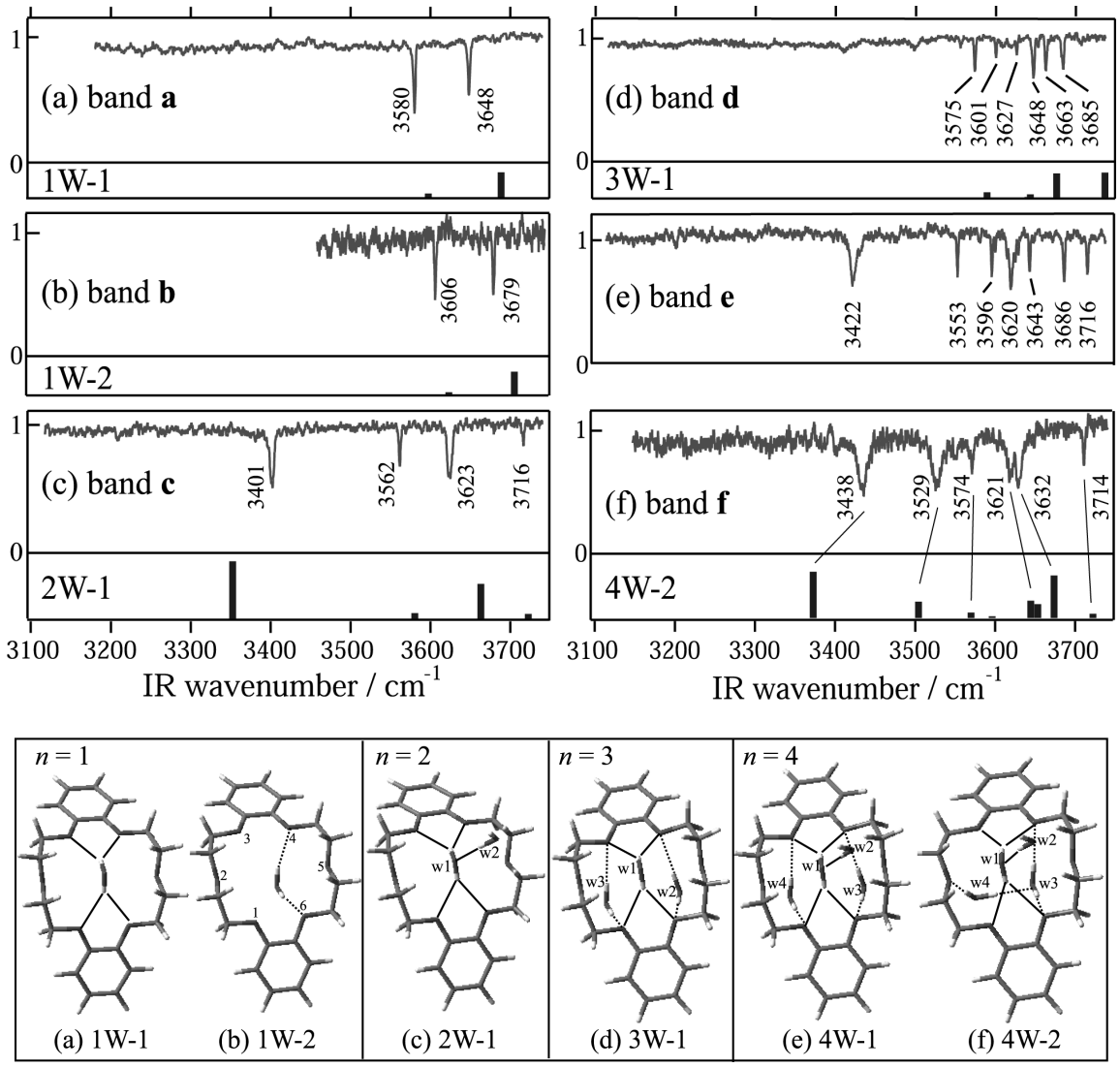

Figure 4 (Upper) (a)-(f) IR-UV DR spectra of DB18C6-$(H_2O)_n$ measured by monitoring bands **a**-**f** in the LIF spectrum, respectively. Sticks under the IR-UV DR spectra denote the calculated IR spectra at the optimized structures. (Lower) Geometric features deduced from the analysis of the IR-UV DR spectra in the OH stretching region of species **a**-**f** of the DB18C6-$(H_2O)_n$ complexes. Figure adapted from (Ref. 47)

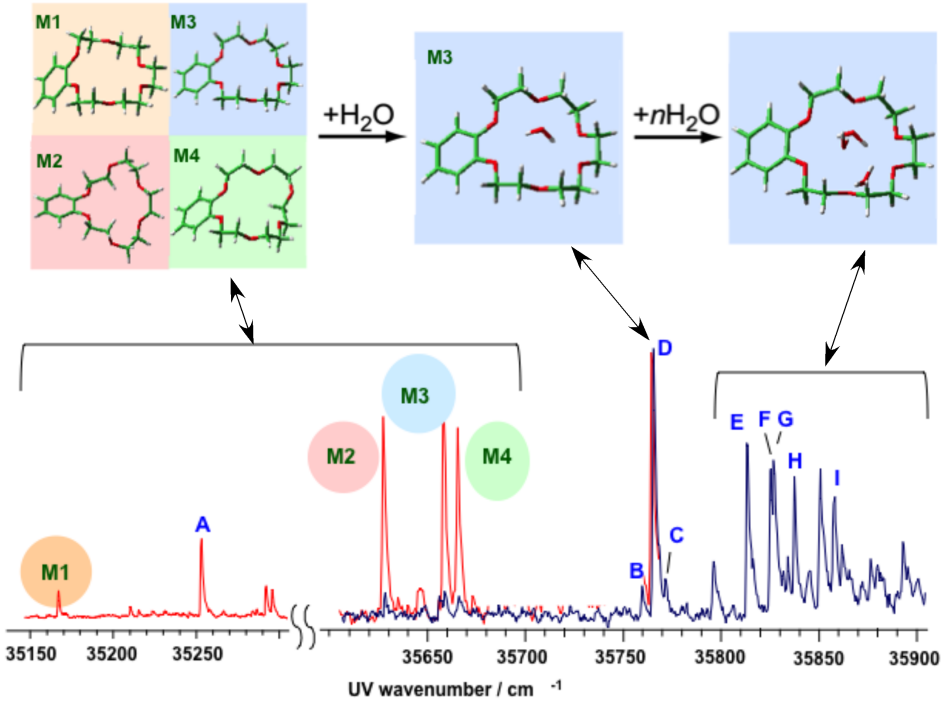

Figure 5 (Upper)Conformer preference for forming B18C6-$(H_2O)_n$ complexes. (Lower) S_1-S_0 LIF spectrum of jet-cooled B18C6 without (red) and with adding water vapor (blue) to the sample gas. M1~M4 are the band origins of different conformers of B18C6 monomer. A~D are due to the different isomers of B18C6-H_2O complex. E~I are due to the B18C6-$(H_2O)_{n>1}$ complexes with B18C6 conformation the same as that of D.

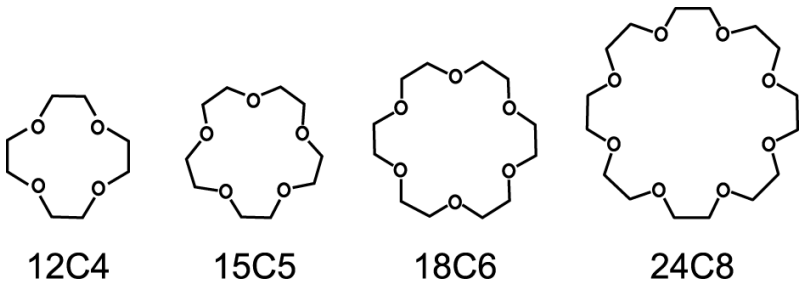

Scheme 2

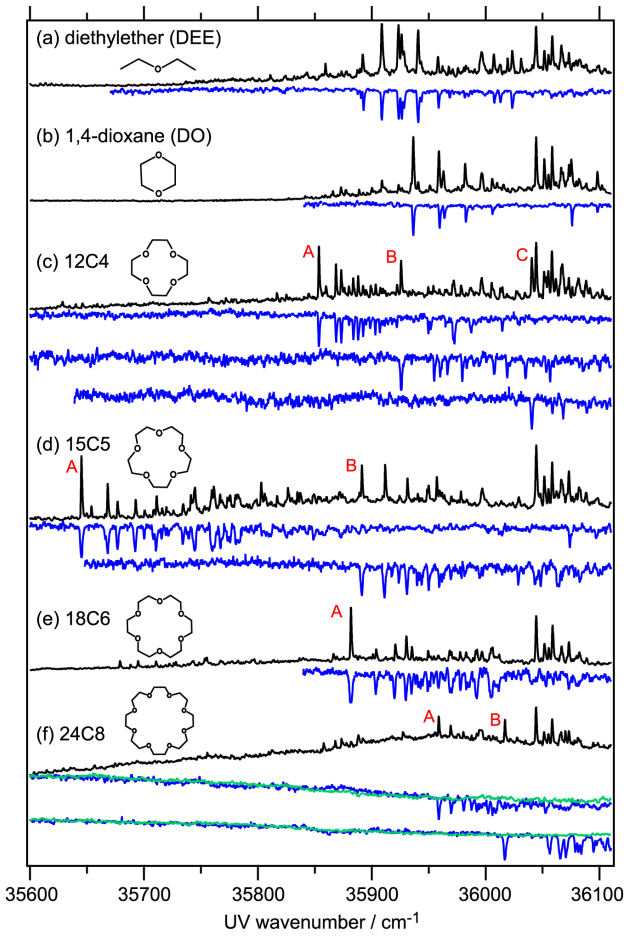

Figure 6. LIF (black) and UV-UV HB (blue and green) spectra of various ether–phenol complexes. Green spectra for 24C8 were obtained by fixing probe UV frequency to positions near bands A and B. Figure adapted from (Ref. 52).

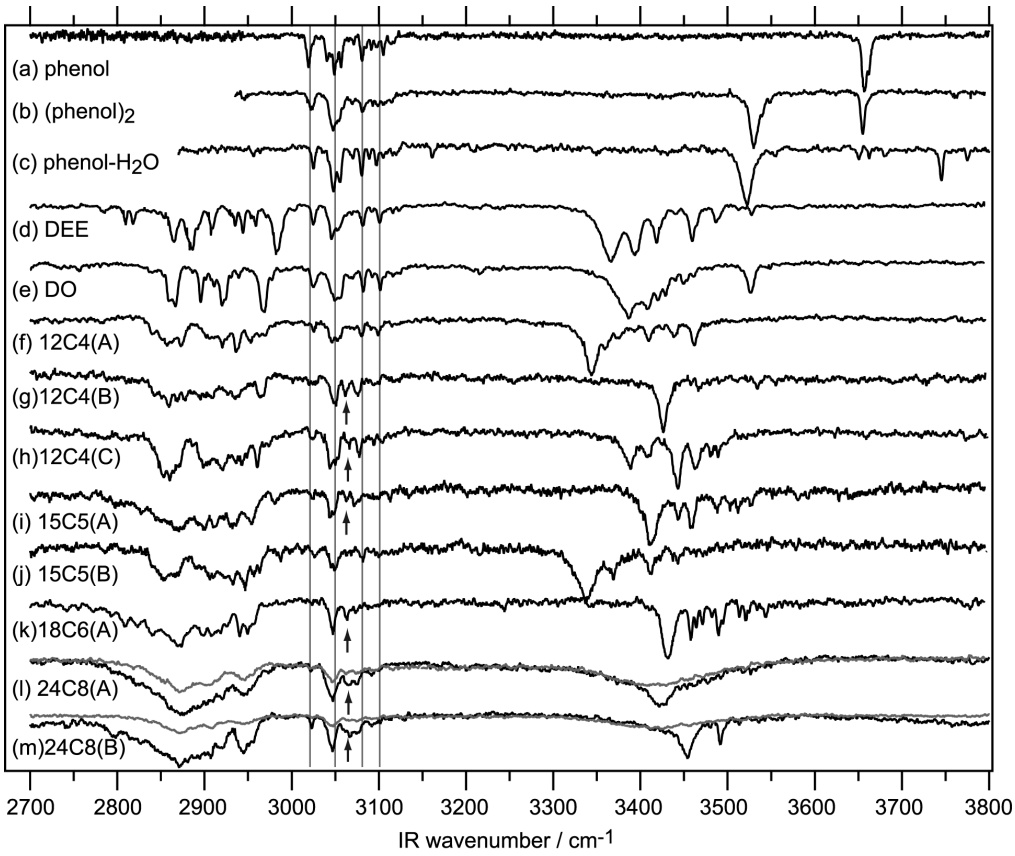

Figure 7. IR-UV DR spectra of (a) phenol, (b) $(phenol)_2$, (c) phenol-H_2O, and (d)-(m) ether-phenol complexes. The gray spectra for 24C8 were obtained by fixing probe UV frequency to positions near bands A and B. Figure adapted from Ref. 52.

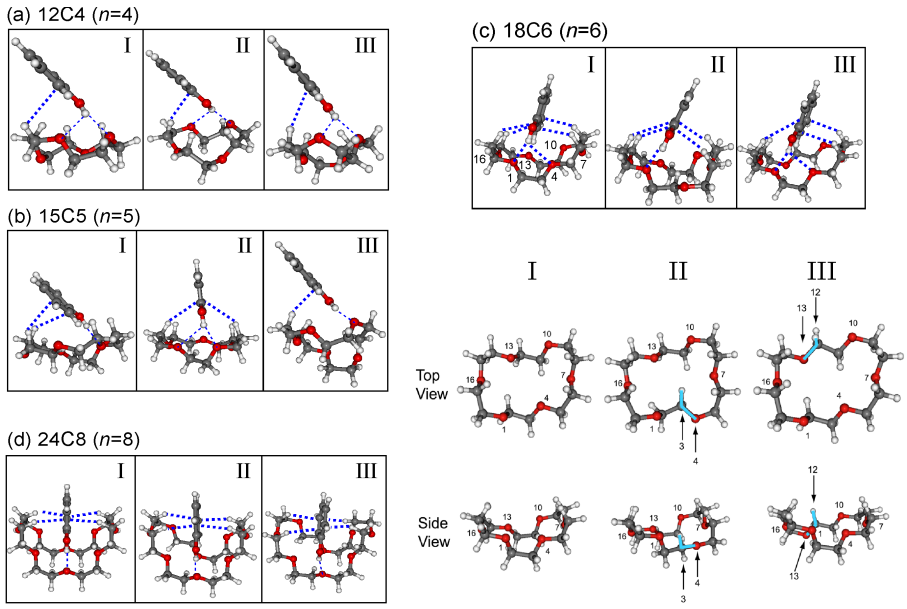

Figure 8. Three most stable isomers of (a)12C4-phenol, (b)15C5-phenol (c)18C6-phenol, and (d)24C8-phenol complexes optimized at the ωB97X-D/6-31++G** level. (Lower panel of (c)) Conformations of 18C6 part of the 18C6-phenol complexes (I), (II) and (III). Figure adapted from Ref. 52.

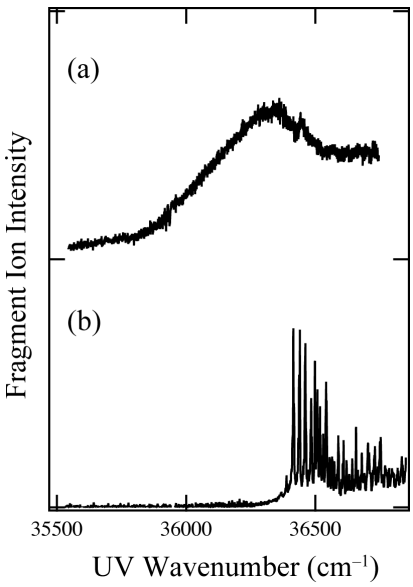

Figure 9. The UVPD spectra of (a) uncooled K^+•DB18C6 and (b) K^+•DB18C6 that is cooled in the 22-pole ion trap. The temperature of the cooled complex is estimated to be ~10 K. Figure adapted from ref. 42.

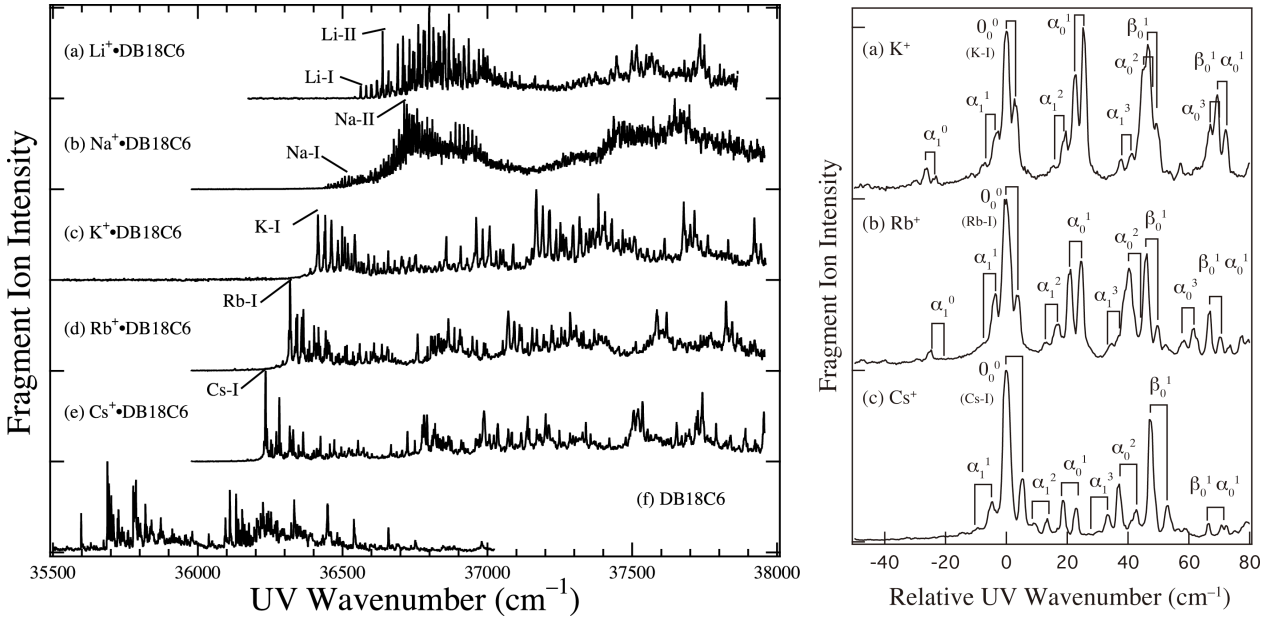

Figure 10. (Left) The UVPD spectra of the M^+•DB18C6 (M = Li, Na, K, Rb, and Cs) complexes with the LIF spectrum of jet cooled DB18C6 reported by Kusaka et al. (Ref. 28). (Right) The UVPD spectra of the DB18C6 complexes with K^+, Rb^+, and Cs^+ around their respective origin bands. The horizontal axis is the UV wavenumber relative to the band origin. The doublet structure connected by solid lines is attributed to the exciton splitting due to the intramolecular interaction between the benzene rings. The low-frequency vibrations appearing in these spectra are labeled by α and β. Superscript and subscript integers with α and β denote quantum numbers of these vibrations in the S_1 and S_0 states, respectively. Figure adapted from ref. 42.

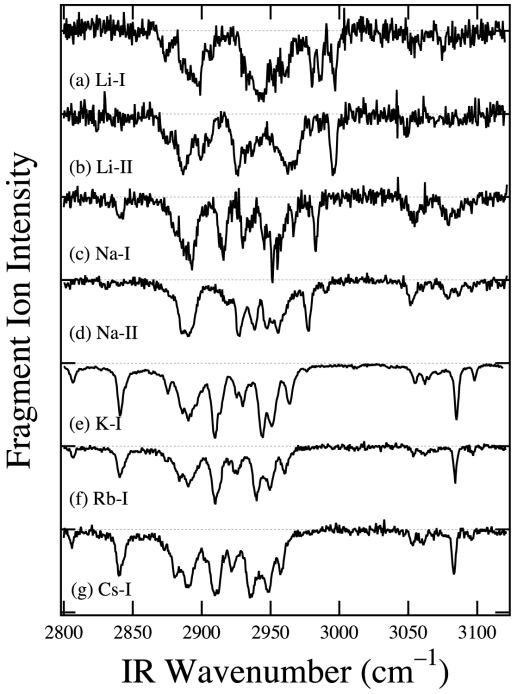

Figure 11. The IR-UV double-resonance spectra of the $M^+ \cdot$DB18C6 (M = Li, Na, K, Rb, and Cs) complexes in the CH stretching region. Figure adapted from ref. 42.

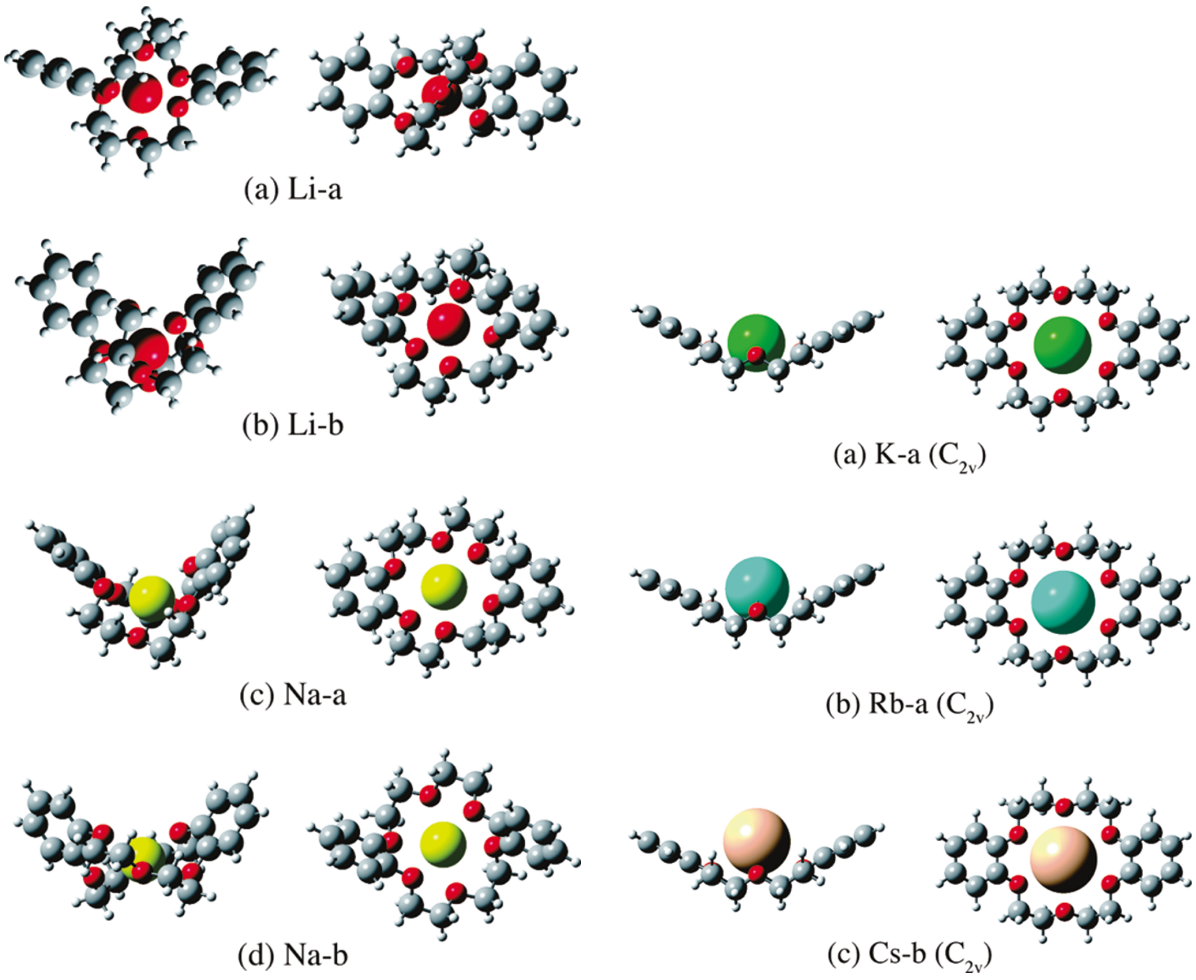

Figure 12. (Left) Structure of (a, b) Li^+•DB18C6 and (c, d) Na^+•DB18C6 complexes optimized at the M05-2X/6-31+G(d) level of theory. (Right) Structure of (a) K^+•DB18C6, (b) Rb^+•DB18C6, and (c) Cs^+•DB18C6 complexes optimized at the M05-2X/6-31+G(d) level of theory. Figure adapted from ref. 42.

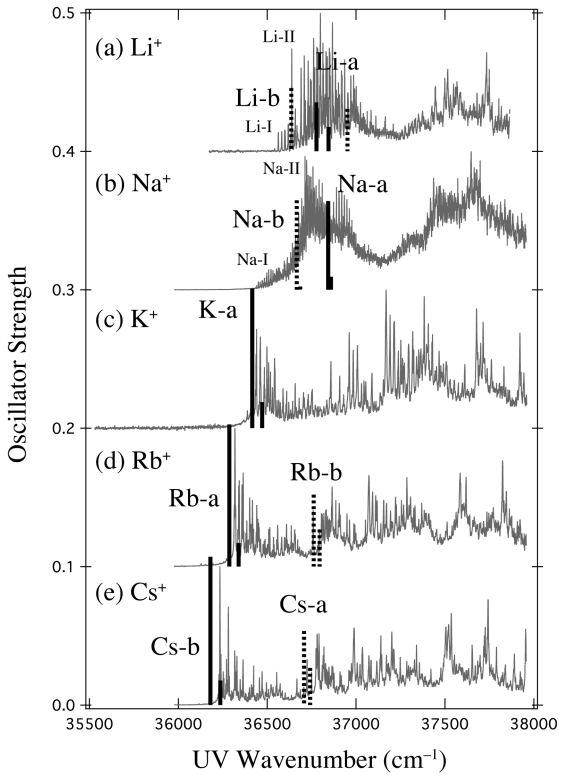

Figure 13. Comparison of the UVPD spectra and the oscillator strengths of electronic transitions for M^+•DB18C6 (M = Li, Na, K, Rb, Cs) calculated with TD-DFT at the M05-2X/6-31+G(d) level and the Stuttgart RLC potential for Rb and Cs. Calculated transition energies are scaled with a scaling factor of 0.8340. Figure adapted from ref. 42.